Journal of applied research and technology
ISSN: 1665-6423
Universidad Nacional Autónoma de México, Instituto de Ciencias Aplicadas y Tecnología

Martínez-Vieyra, C.; Olguin, M. T.; Gutiérrez-Segura, E.; López-Tellez, G.

Comparison of Ag, Cu and Zn nanoparticles obtained using *Aloe vera* extract and gamma ionizing radiation

Journal of applied research and technology, vol. 18, no. 5, 2020, pp. 289-314
Universidad Nacional Autónoma de México, Instituto de Ciencias Aplicadas y Tecnología

DOI: https://doi.org/10.14482/INDES.30.1.303.661

Available in: https://www.redalyc.org/articulo.oa?id=47471674006

Journal of Applied Research and Technology

www.jart.icat.unam.mx

Journal of Applied Research and Technology 18 (2020) 289-314

Original

Comparison of Ag, Cu and Zn nanoparticles obtained using *Aloe vera* extract and gamma ionizing radiation

C. Martínez-Vieyra[a] • M. T. Olguin[b]* • E. Gutiérrez-Segura[c] • G. López-Tellez[c]

[a]*Universidad Autónoma del Estado de México, Facultad de Química, Doctorado en Ciencia de Materiales. Toluca, México*
[b]*Instituto Nacional de Investigaciones Nucleares, Departamento de Química. Ocoyoacac, México*
[c]*Universidad Autónoma del Estado de México, Facultad de Química. Toluca, México*
[d]*Universidad Autónoma del Estado de México-Universidad Nacional Autónoma de México, Centro Conjunto de Investigación en Química Sustentable. Tlachaloya, México*

Received 11 14 2019; accepted 09 29 2020
Available online 10 31 2020

Graphical abstract

The precursor to obtaining metallic nanoparticles and the route of synthesis define the purity, morphology, crystallinity, and chemical speciation of the metal.

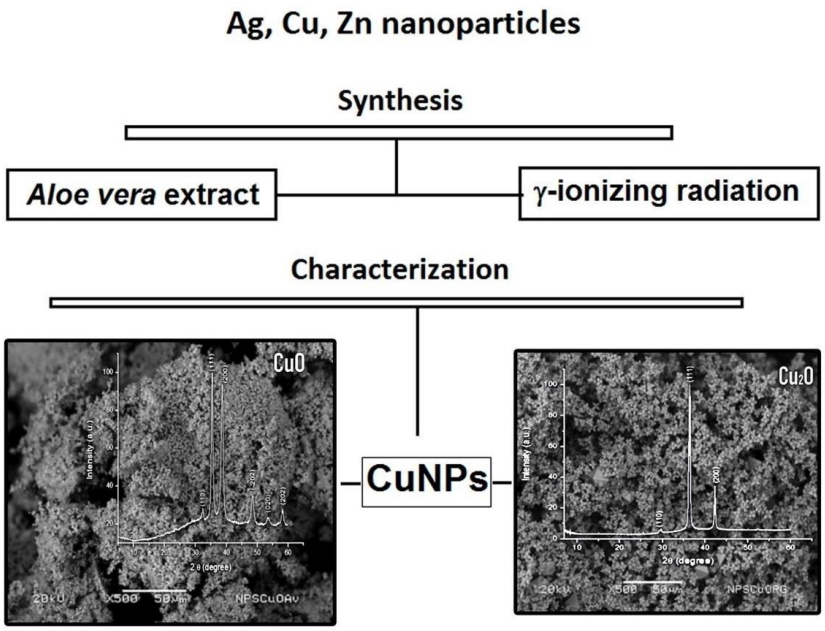

Highlights

- Phytochemicals and ionizing radiation determine the morphology of nanoparticles.
- *Aloe vera* extract and gamma irradiation influence the size of nanoparticles.
- Gamma irradiation (0.756 kGy/h) is efficient in the production of Ag and Cu_2O nanoparticles.
- The counterion is important when obtaining Cu_2O nanoparticles by gamma radiation.
- The copper oxidation state in the CuNPs depends on the synthesis method.

Abstract: The characteristics of the nanoparticles of silver, copper and zinc obtained from two synthetic routes were investigated. A possible future application of these nanoparticles is as bactericidal agents. The reduction methods were *Aloe vera* extract and gamma ray irradiation with a dose rate of 0.756 kGy/h and a total dose of 40 kGy from a ^{60}Co-source. The chemical species of the nanoparticles (NPs) obtained by *Aloe vera* extract were Ag, CuO, and ZnO; while the NPs obtained using gamma irradiation were Ag and Cu_2O. The precursor to obtaining the nanoparticles and the route of synthesis define the purity, morphology, crystallinity, and chemical speciation of the metal.

Keywords: metallic nanoparticles, *Aloe vera*, gamma irradiation, chemical speciation, nanoparticle sizes

*Corresponding author.
E-mail address: teresa.olguin@inin.gob.mx (M. T. Olguin).
Peer Review under the responsibility of Universidad Nacional Autónoma de México.

1. Introduction

During recent decades, metallic and oxide metallic nanoparticles, including silver (Ag) (Brabazon et al., 2017), copper oxides (CuO, Cu_2O) and zinc oxide (ZnO) (Alswat, Ahmad, & Saleh, 2017) have grown in importance as a consequence of their small size (1-100 nm). They exhibit an upper surface area to volume ratio. This fact improves the physicochemical properties in comparison with those of the same material in bulk (Dizaj, Lotfipour, Barzegar-Jalali, Zarrintan, & Adibkia, 2014).

Among noble metal nanoparticles, Ag NPs have been the object of the attention of many researchers due to their particular characteristics, such as good conductivity, chemical stability, catalytic (Khodadadi, Bordbar, Yeganeh-Faal, & Nasrollahzadeh, 2017), and antimicrobial properties (Hajipour et al., 2012). Silver nanoparticles have been used in a lot of products including clothing (Mohanbaba & Gurunathan, 2016), textiles (Emam, El-Rafie, Ahmed, & Zahran, 2015), food packaging (Williams, Valencia, Gokulan, Trbojevich, & Khare, 2017), electronic components (Ahmed, Ahmad, Swami, & Ikram, 2016), as well as water disinfection systems (Tran, Nguyen, & Le, 2013), and the health industry (wound dressing, dental hygiene, catheters) (Yah & Simate, 2015). The typical plasmon absorbance features that Ag NPs present have been used in the fabrication of chemical sensors and biosensors (Unser, Bruzas, He, & Sagle, 2015).

Copper (Cu) is a more abundant and cheaper element than silver and, similarly to gold, is considered one of the noble metals. However, Cu has better electrical and optical properties than other metallic species (Hori, Nagata, Iwase, & Hori, 2014). Copper oxide (CuO) has a monoclinic crystalline structure, and it is a transitional metal oxide. Nanoparticles of this compound are stable in a mixture with polymers or macromolecules (Ingle, Duran, & Rai, 2014). Nanoscale materials have shown different and improved properties. For example, CuO NPs are more catalytically active than the same compound in bulk (Wang, Wang, Yan, Chen, & Song, 2016). According to the shape, size and composition of the copper oxide nanoparticles, they could present several practical properties (Kumar, Smita, Cumbal, Debut, & Angulo, 2017). They have been considered in materials for gas sensors (Wang & Hu, 2009), dye sensitized solar cells (Baqer et al., 2018), in waste water treatment (catalytic degradation textile dye) (Sharma et al., 2018), and in agriculture (Kasana, Panwar, & Kaul, 2017). They are used in filters, textiles (Bashiri, Majid, Mahnaz, & Rad, 2018) and food packaging too (El-Batal, El-Sayyad, El-Ghamery, & Gobara, 2017) due to their antimicrobial properties (Ahamed & Alhadlaq, 2014).

Zinc oxide is an important semiconductor material (Mahendiran et al., 2017). It is cheap, readily available, and innocuous to the environment (Elumalai, Velmurugan, Ravi, Kathiravan, & Adaikala Raj, 2015). Besides, due to a large exciton binding energy of 60 meV, it has potential applications in optoelectronic devices, such as solar cells (Sutradhar & Saha, 2015). Zinc Oxide (ZnO) nanoparticles have a large specific surface area. This characteristic significantly increases the efficiency of these nanoparticles for several applications, such as UV radiation blocking (Sricharussin, Threepopnatkul, & Neamjan, 2011). Zinc oxide nanoparticles have long been known for their antibacterial and antifungal properties (Siddiqi, ur Rahman, Tajuddin, & Husen, 2018). They are also used in catalytic water treatment (Farzaneh, Asgharpour, Nouroozi, & Haghshenas, 2017) and for agricultural purposes (Singh, 2018).

The use of plants (Mohanbaba & Gurunathan, 2016; Kumar, Venkatesh, Bhowmik & Kuila 2018), their parts (Patil & Taranath, 2018) or agro waste materials (Chikkanna, Neelagund, & Rajashekarappa, 2019) in order to obtain nanoparticles rather than using chemical techniques is notable because there are no hazardous chemicals which can be adsorbed on the nanoparticle's surface. These can lead to adverse effects on pharmaceutical and biomedical applications. In the biosynthesis of NPs using plants, some biomolecules act as reducing agents and others are capping agents for the resulting nanoparticles nucleus, as mentioned by Venkatesh et al. (2015). Therefore, this method is nontoxic, facile, sustainable and can be scaled up for a lower cost.

Aloe vera is native of North Africa, but today is common in several countries around the world. It grows easily in warm and tropical areas. It is 99 – 99.5% water and the remaining material (1-0.5%) contains over 75 biologically active ingredients such as vitamins, minerals, enzymes, sugars, anthraquinones or phenolic compounds, amino acids (Watson & Zibadi, 2013), heterocyclic and carbonyl compounds. That is why this plant and its gel have been used in health, beauty, and medicine for 2000 years (Surjushe, Vasani, & Saple, 2008). Nowadays, the aqueous extract of *Aloe vera* is employed to elaborate nanoparticles too (Venkatesh et al., 2015). This is due to the presence of benzoquinones, which act as reducing agents in the formation of nanoparticles (Figure 1). Amino acids (among them arginine, histidine, lysine, aspartic and glutamic acid) and proteins, on the other hand, regulate the form and size of nanoparticles by the weak binding of incipient nanocrystals (Zhang et al., 2010).

The use of radiation, especially gamma irradiation is another interesting method for producing metal and metal oxide nanoparticles (Gerasimov, 2011). Gamma irradiation provides a high level of purity in the obtained nanomaterials (Kamil Othman, Abdul Hamid, Saion, Abedini, & Daud, 2013). When gamma radiation interacts with water, different kinds of agents (reducers and oxidants) are obtained (equation 1). Inside these species, there are two more important aspects: i) solvated electrons, which present reductive characteristics,

with E_o= -2.87 V, and ii) the H• radical with E_o= -2.3 V, as reported by Rojas and Castano (2012). Both reducers can interact with metal ions and promote atoms M° with zero valances (equations 2 and 3). Clifford, Castano, and Rojas (2017) reported that this reduction reaction could be complicated because the ions could be reduced to intermediate valence states. The atom will tend to dimerize, or it will interact with ions to form nucleation points, which will grow into particles to produce a high number of reduced species. It is recommended that before irradiation, the metallic precursor solution be added along with a few milliliters (mL) of secondary alcohol (isopropanol) or formate anion solution. This acts as a scavenger of oxidizer species, especially hydroxyl radical OH• (Flores-Rojas, López-Saucedo, & Bucio, 2018), and possesses a strong oxidation potential of E_o=+2.73 V and brings ions to a higher oxidation state.

$$H_2O \xrightarrow{\text{gamma radiation}} e_{aq}^-, H_3O^+, H^\bullet, H_2, OH^\bullet, H_2O_2 \quad (1)$$

$$M^+ + e_{aq} \longrightarrow M^\circ \quad (2)$$

$$M^+ + H^\bullet \longrightarrow M^\circ + H^+ \quad (3)$$

Metallic nanoparticles have been obtained from plant extracts. Patil and Taranath (2018) synthesized silver and zinc oxide nanoparticles using leaf extract of *L. acidissima*. They found a characteristic surface plasmon resonance (SPR) at 452 and 374 nm, respectively. Besides, both presented spherical morphology with sizes from 21 to 42 nm and 12 to 53 nm, respectively. The extract of *R. graveolens* was used to synthetize zinc oxide nanoparticles, which present microbicidal and oxidant properties. The XRD patterns confirmed the presence of a hexagonal Wurtzite structure with a particle-size range of 20 to 30 nm, according to the results obtained by Lingaraju et al. (2016). *Prunus serotina* cherry extract has also been used for the synthesis of silver nanoparticles with a spherical shape and a diameter of 20-80 nm. These presented a characteristic UV-Vis absorption peak at 425 nm (Kumar, Angulo, Smita, Cumbal, & Debut, 2016). Ghidan, Al-Antary, & Awwad, (2016) have reported that *Punica granatum* peel extract was useful in obtaining nanoparticles of copper oxide. In this case, the absorbance peak was near 282 nm, and the nanoparticles exhibited spherical morphology and an average size of 40 nm.

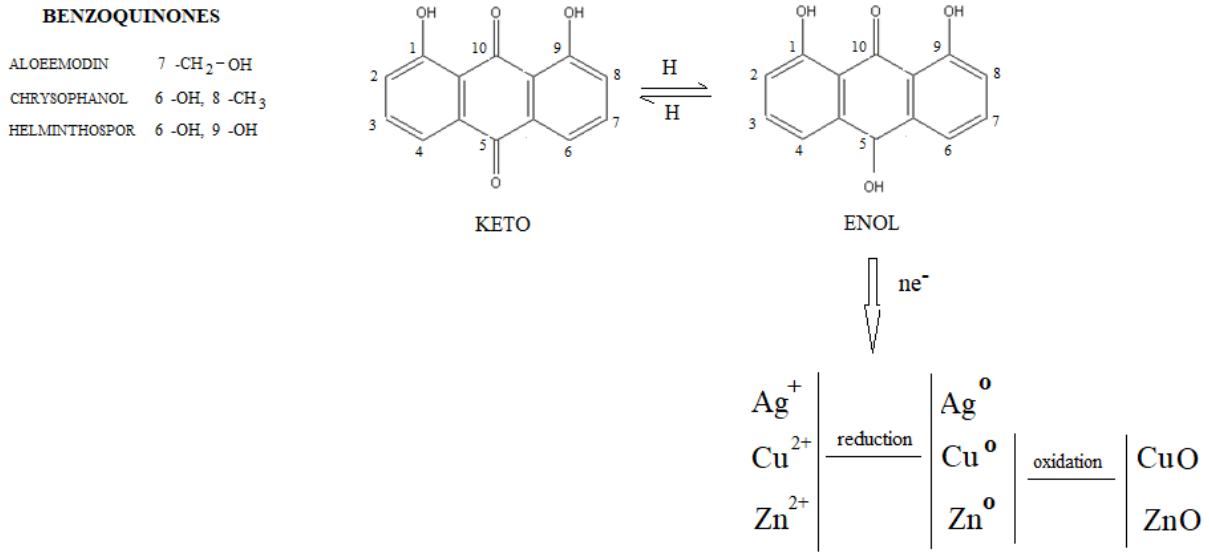

Figure 1. Reduction mechanism with Aloe vera.

Gamma irradiation is a powerful tool for producing metal nanoparticles in aqueous media because reducing chemical agents are not necessary and no by-products are generated during the exposure process. Hori et al. (2014) fabricated copper nanoparticles using 20 kGy (total dose) at 4.70 kGy/h (dose rate). The particle was 13 nm in size and spherical in shape. UV-Vis spectra showed a peak near 370 nm, assigned to the nanoparticles of Cu_2O, which have a cubic crystal system. In a similar way, Sheikh, Akhavan, and Kassaee (2009) obtained silver nanoparticles which were about 16 nm in size by way of a cubic crystal system, using a Gammacell 220 facility with 18.6 Gy/h.

Therefore, based on the importance of the synthesis route in obtaining metallic nanoparticles with specific characteristics (morphology, sizes, crystallinity, chemical speciation and purity), the aim of this work was to obtain silver, copper or zinc nanoparticles through green and non-conventional routes under different experimental conditions. The characteristics of the nanoparticles obtained were compared to visualize their possible use as bactericidal agents.

2. Materials and methods

2.1. Materials and equipment

Aloe vera leaves were purchased from the Morelos market in Toluca, Mexico. ACS grade silver nitrate ($AgNO_3$), copper acetate $Cu(CH_3COO)_2{\cdot}H_2O$ were purchased from Merck Chemicals. Copper nitrate hemipentahydrated ($Cu(NO_3)_2{\cdot}2.5H_2O$) and zinc nitrate hexahydrate ($Zn(NO_3)_2{\cdot}6H_2O$) were procured from Sigma-Aldrich Chemicals. Isopropanol was supplied by Tecsiquim S.A. de C.V. Gamma irradiation was carried out using an irradiator LGI-01 Transelektro and facilitated by the National Institute for Nuclear Research (Mexico).

The colloidal solutions of NPs obtained were separated using a centrifuge (model Dorolab CN-CH4). Following the generation of the zinc nanoparticles (ZnNPs) by the biological route (extract of *Aloe vera*), the intermediate sample was annealed using a furnace (model 62700 Barnstead Thermolyne). The UV-Vis analysis was recorded by the Thermo Scientific Genesys 10S double beam spectrophotometer, from 200-700 nm. The morphology of the nanoparticles as well their composition was determined by Scanning Electron Microscopy (SEM) and X-ray Energy Dispersive Spectroscopy (EDS), using a JEOL model JSM-5900LV with a DX-4. The morphology and size of synthesized NPs were observed and captured with a Transmission Electron Microscopy (TEM) JEOL model JEM-2010, operating at 120 kV accelerating voltage, equipped with a camera, (model ORCAFLASH40CHAM). Sample preparation was done by suspending NPs in ethanol and sonicating them for 5 min. A drop of this suspension was placed on a grid of carbon-coated copper. Only in the case of CuNPs, was a carbon-coated nickel grid used. A D8 Discover diffractometer was used to record the X-ray diffraction patterns (XRD) of the samples, with Cuα radiation (λ= 1.5406 Å). The scanning was done in the region of 4°- 60° 2θ. The X-ray photoelectron spectroscopy analysis (XPS) was carried out with Thermo Scientific model K-Alpha.

2.2. Biological synthesis

2.2.1. Extract preparation of Aloe vera leaves

The *Aloe vera* leaves were washed with drinking water and dried using a clean rag, and then, 30 g of leaves were finely chopped, and 250 mL of distilled water was added. The mixture was boiled for 10 min. After, the mixture was left to cool to room temperature. The resultant solution was decanted and filtered using a Whatman® Grade 1 qualitative filter paper. Finally, the *Aloe vera* extract was kept in reserve at 4 °C as a stock solution.

2.2.2. Synthesis of Ag, Cu and Zn nanoparticles

One mL of 30% ammonia solution was discharged into a 100 mL Erlenmeyer flask containing an aliquot of 5 mL of $AgNO_3$ 10 mM solution. Next, 5 mL of *Aloe vera* extract were added under constant agitation at room temperature. Water was added until a final volume of 50 mL was reached. After 24 h (isolated from light), the reaction mixture acquired a faint yellow color. Afterward, the mixture was separated by centrifugation at 6000 rpm for 10 min (twice). The precipitate was washed two times with distilled water and then with ethanol, finally it was dried in an oven at 50 °C for 2 h (Chandran, Chaudhary, Pasricha, Ahmad, & Sastry, 2006).

Five milliliters of *Aloe vera* extract were added to a 100 mL flat-bottom ball flask containing 50 mL of $Cu(NO_3)_2{\cdot}2.5H_2O$ 10 mM solution with constant stirring. Then, the reaction mixture was refluxed for 24 h. While the reaction progress, a color change (from blue to brown) was noted. The obtained dark solution was separated by centrifugation at 6000 rpm for 12 min to complete the precipitation of CuNPs. The black color observed in the CuNPs was washed away with distilled water and ethanol respectively, and then dried at room temperature (Kumar et al., 2018).

One point five grams of zinc nitrate hexahydrate $Zn(NO_3)_2{\cdot}6H_2O$ was dissolved in 20 mL of distilled water. Then, the solution was added dropwise to a 100 mL flat-bottom ball flask containing 30 mL of *Aloe vera* extract. Finally, 1 mL of 30% ammonia solution was added to adjust the pH of the medium, with vigorous stirring at room temperature. After 6 h, the resulting white precipitate was centrifuged at 6000 rpm for 10 min, the supernatant was removed, and the sediment was re-dispersed with distilled water and centrifuged once again. The sediment was recovered and air-dried in an oven at 60°C for 4 h. The obtained solid was annealed in a furnace at 380°C for 2 h (Elumalai et al., 2015).

The different materials obtained by this green synthesis were named AgNPsAv, CuNPsAv and ZnNPsAv, respectively.

2.3. Gamma irradiation shyntesis

Fifteen mL of every metal precursor solution (0.1 M $AgNO_3$; 0.1 M $Cu(CH_3COO)_2$. H_2O) were placed in a corresponding 25 mL flask. Then, 1 mL of isopropanol was added to each one. The flask was covered using septum, after each solution bubbled with highly pure nitrogen for 10 min. The resultant solutions were sealed and irradiated in ambient conditions with ^{60}Co γ-rays source at a dose rate of 0.756 kGy/h and a total dose of 40 kGy. The different materials obtained were named AgNPsγ and CuNPsγ. It is important to mention that the ZnNPs was not obtained under the experimental conditions established for this purpose.

3. Results and discussion

3.1. NPs obtained with Aloe vera extraction

3.1.1. AgNPsAv

EDS analysis shows the chemical composition of Ag nanoparticles with a weight percent of 65.98±25.23% for Ag, but this analysis exhibits weak signals from C, O, Mg, P and Ca too. These signals may be due to the organic macromolecules present in the *Aloe vera* extracts (Figure 2a). Besides, TEM micrograph (Figure 2b) shows a spherical shape distribution of Ag NPs, with sizes from 2 to 40 nm, and the corresponding histogram of particle size distribution with an average size of 14.0 nm (±9.5), Figure 2c. The absorption spectra (Figure 2d) exhibit a broad peak at 390-450 nm, which corresponds to the characteristic surface plasmon resonance (SPR). As mentioned by Tan and Cheong (2013), if the peak is broad, it means that the size distribution of nanoparticles obtained is widespread. Singh, Bharti, and Meena (2015) explain that the size-dependence of SPR peak position is the result of a size-dependent effective dielectric constant of a metal particle at the nanoscale. The electrons are scattered on the particle surface, leading to changes in this constant due to electromagnetic interaction between neighboring particles. The XRD pattern of synthesized AgNPsAv (Figure 2e) presents two reflections at 38.14° 2θ and 44.32° 2θ, assigned to [111] and [200] planes respectively (PDF 89-3722). These reflections correspond to face-centered cubic silver (FCC). However, impurities were detected in the form of a reflection at 13.40° 2θ. These could be *Aloe vera* extract components like proteins, amino acids, carbohydrates and phenolic compounds, among others. These act as capping agents because they have acids and carbonyl functional groups that could compensate the Van Der Waals forces between particles which could generate a negative charge around AgNPsAv (Singh, et al., 2015; Logaranjan, Raiza, Gopinath, Chen, & Pandian). The signals at binding energies of XPS spectra (Figure 2f) of 368.5 eV and 374.4 eV correspond to the $3d_{5/2}$ and $3d_{3/2}$ orbitals of Ag(0) (metallic silver). This is similar to what was reported by Sharma, Dhillon, and Kumar (2018).

3.1.2. CuNPsAv

EDS results confirm the chemical composition of the synthesized CuNPsAv, with weight percent of 93.33±2.06 for copper and 6.66±2.06% for oxygen; while (Figure 3a) TEM images (Figure 3b) denote a spherical morphology and the histogram of the particle size distribution of CuNPs, with a medium of 6.93 nm (± 1.92), Figure 3c. In the corresponding UV-Vis spectrum (Figure 3d), a peak can be observed around 250-300 nm, which suggests the formation of CuO nanoparticles (Zhu et al., 2004), due to the inter-band transition of core electrons of copper metal. This was also reported by Kumar et al. (2017). The reflections observed in the XRD pattern at 32.35°2θ, 35.37°2θ, 38.64°2θ, 48.54°2θ, 54.27°2θ and 58.25° 2θ, were assigned to (110), (111) (200), (-202), (020), (202) and (-113) planes respectively, and no characteristic reflections of any impurities were detected (Ahamed & Alhadlaq, 2014), Figure 3e. According to Wang et al. (2016) reflections can be indexed to the monoclinic structure of CuO nanoparticles, corresponding with PDF 80-1916. XPS spectra analysis (Figure 3f), on the other hand, presents a typical Cu (II) $2p_{3/2}$ binding energy at 934.4 eV and Cu (II) $2p_{1/2}$ 954.3 eV, values separated from 19.9 eV, which is similar to that reported by Kwon et al. (2013).

3.1.3. ZnNPsAv

The EDS analysis of ZnO nanoparticles exhibits signals for zinc (84.90±3.18 wt. %) and oxygen (15.09±3.18 wt. %), similar to those reported by Singh (2018), Figure 4a. Representative TEM images of nanoparticles reveal a spherical morphology shown in Figure 4b. The UV-Vis spectra (Figure 4c) have an absorption peak at 378 nm, which is characteristic of ZnO nanoparticles. Elumalai Velmurugan, Ravi, Kathiravan, and Ashokkumar (2015) attributed this peak to the intrinsic bandgap absorption of ZnO due to the electron transition from the valence band to the conduction band. The powder diffraction pattern (Figure 4d) of the sample exhibits reflections at 31.80°2θ, 34.46°2θ, 36.32°2θ, 47.54°2θ and 56.59°2θ. These can be indexed to (100), (002), (101), (102) and (110) planes, respectively, assigned to a hexagonal Wurtzite structure (PDF 89-1397). The Scherrer equation (Rehana, Mahendiran, Kumar, & Rahiman, 2017) (equation 4) was used to calculate average particle size:

$$D=k\lambda/\beta\cos\theta \quad (4)$$

Where D is the crystallite size in nm, K is the shape factor (0.94), λ is the wavelength of the X-ray (0.154 nm), the full width at half maximum (FWHM) for the main intensity reflection in the diffraction pattern, θ is the Bragg's angle.

The calculated size of ZnO nanoparticles was of 5 nm agreed with TEM images (Figure 4b). The high-resolution Zn 2p XPS spectrum (Figure 4e) consists of two peaks of Zn $2p_{3/2}$ and Zn $2p_{1/2}$, which correspond to 1021.6 eV and 1044.6 eV, respectively. The separation between these two peaks is 23 eV, which is similar to the standard reference value of ZnO (Yu, Wen, Yang, & Cai, 2019)

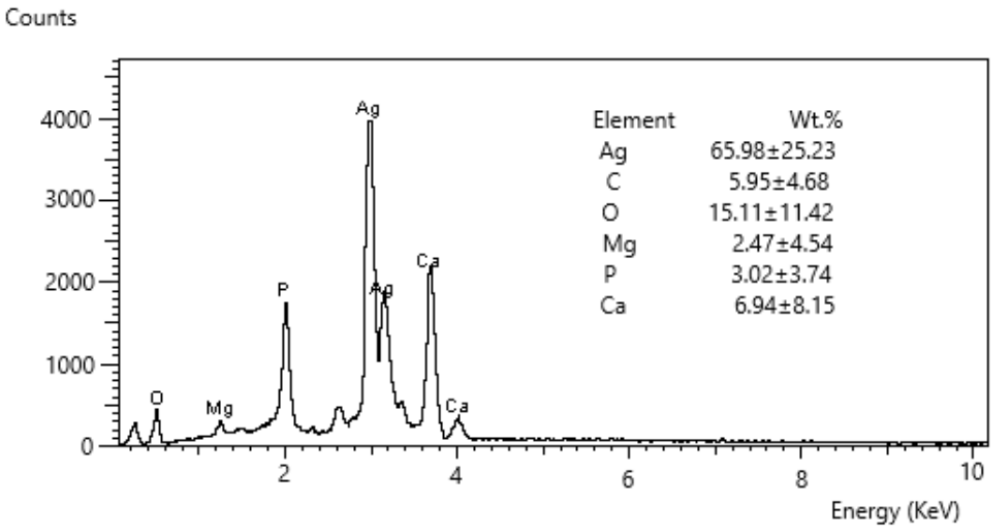

(a)

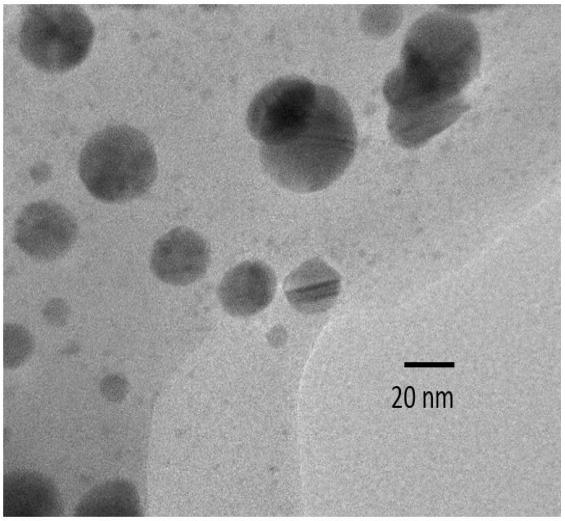

(b)

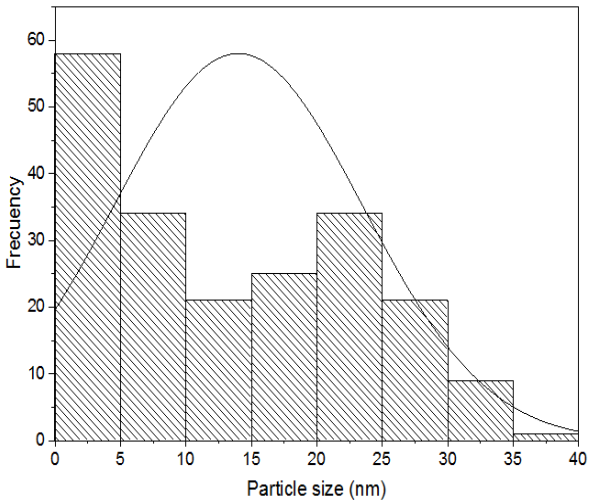

(c)

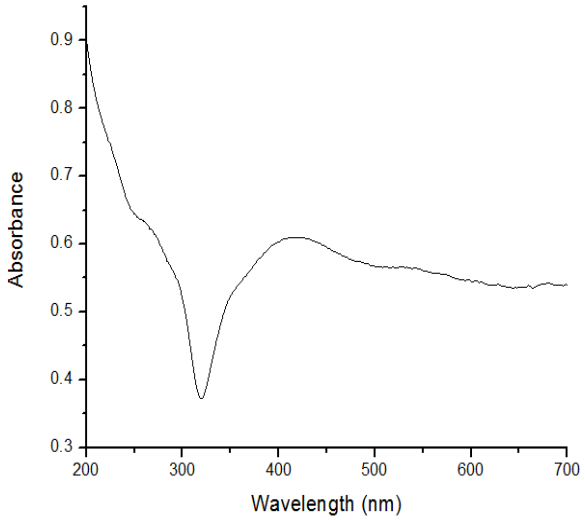

(d)

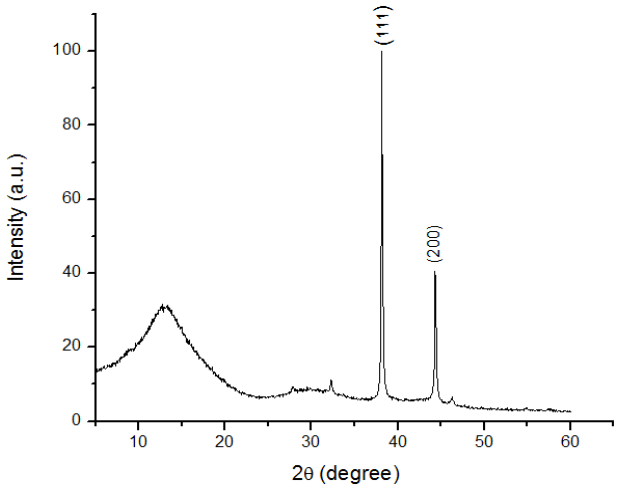

(e)

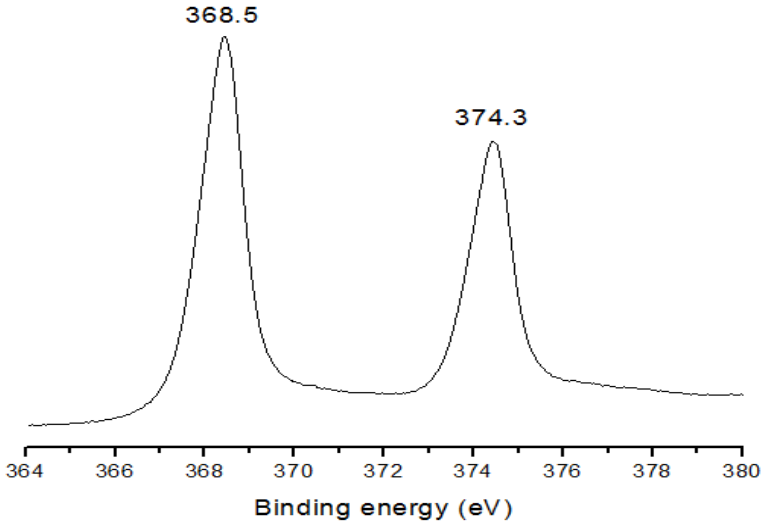

(f)

Figure 2. EDS pattern and wt. (%) of each component
(a), TEM image and histogram of distribution of particle size
(b, c), UV-Vis spectra (d), XRD diffraction pattern
(e), and high resolution XPS spectrum for Ag 3d
(f), of AgNPsAv.

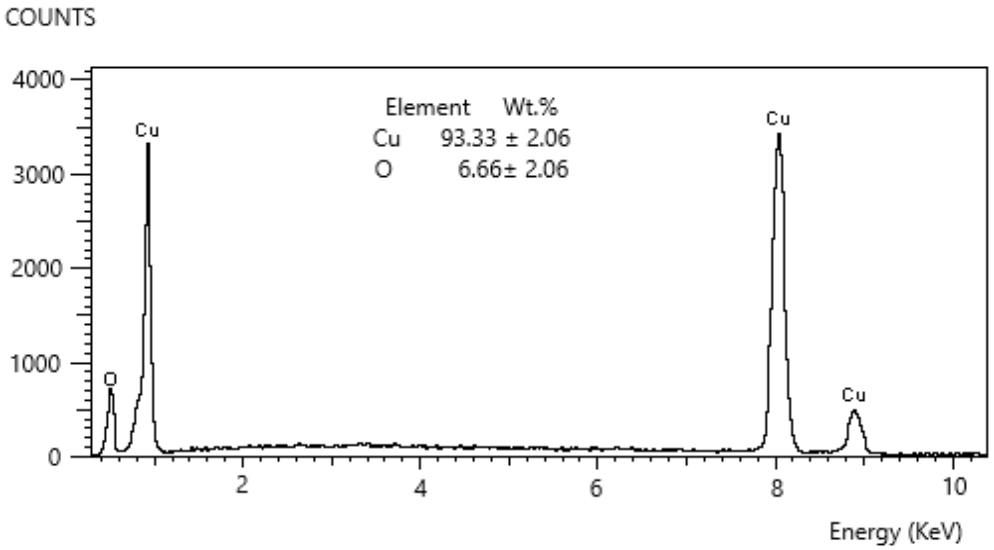
COUNTS
4000
3000
2000
1000
0
Element Wt.%
Cu 93.33 ± 2.06
O 6.66± 2.06
Cu
Cu
Cu
O
2
4
6
8
10
Energy (KeV)

(a)

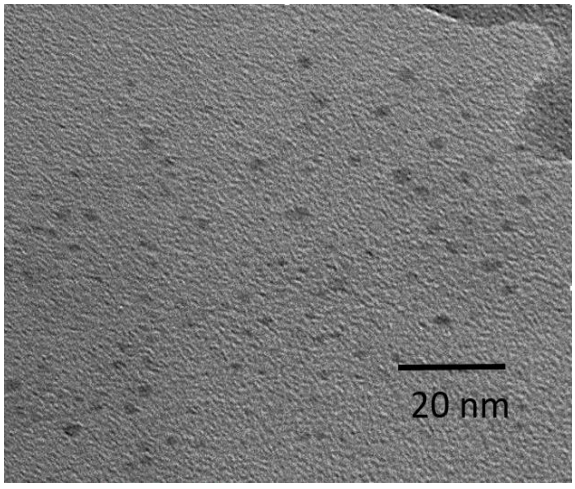
20 nm

(b)

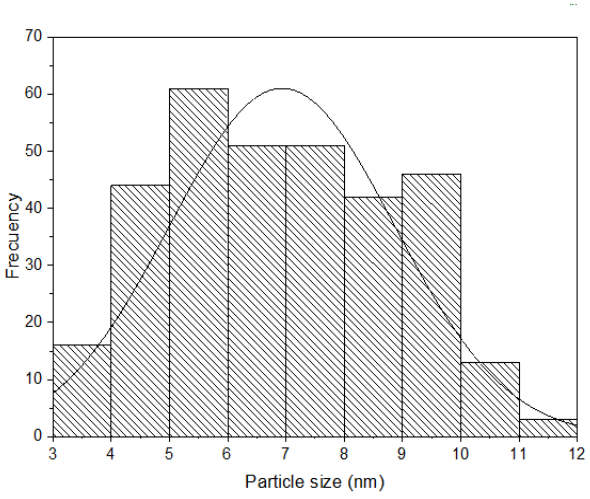
70
60
50
40
30
20
10
0
Frecuency
3
4
5
6
7
8
9
10
11
12
Particle size (nm)

(c)

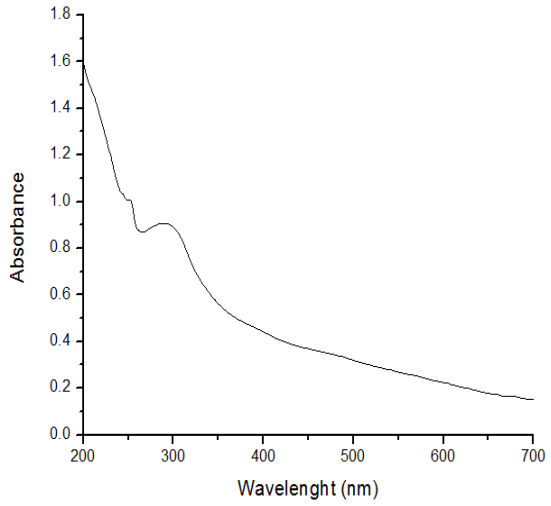

(d)

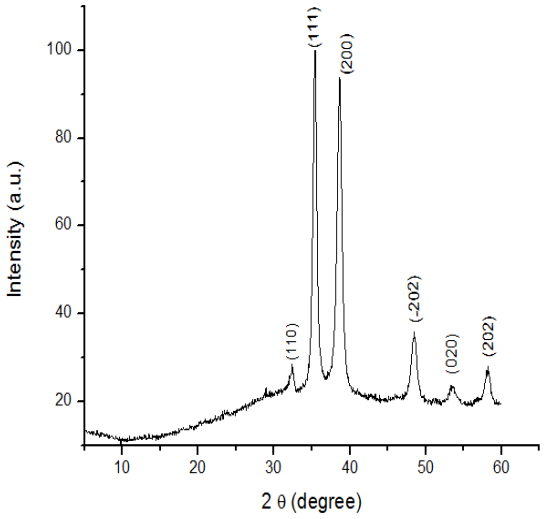

(e)

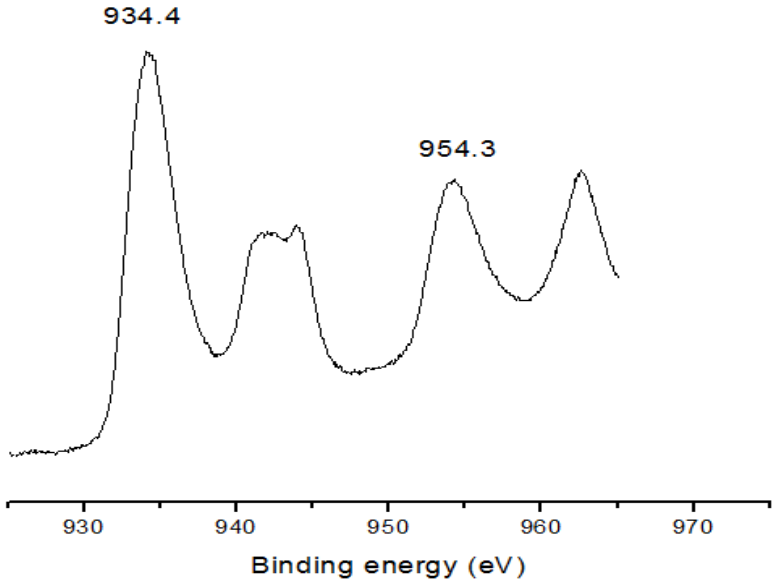

(f)

Figure 3. EDS pattern and wt. (%) of each component
(a), TEM image and histogram of distribution of particle size,
(b, c), UV-Vis spectra (d) XRD diffraction pattern
(e), and high resolution XPS spectrum for Cu 2p
(f), of CuONPsAv.

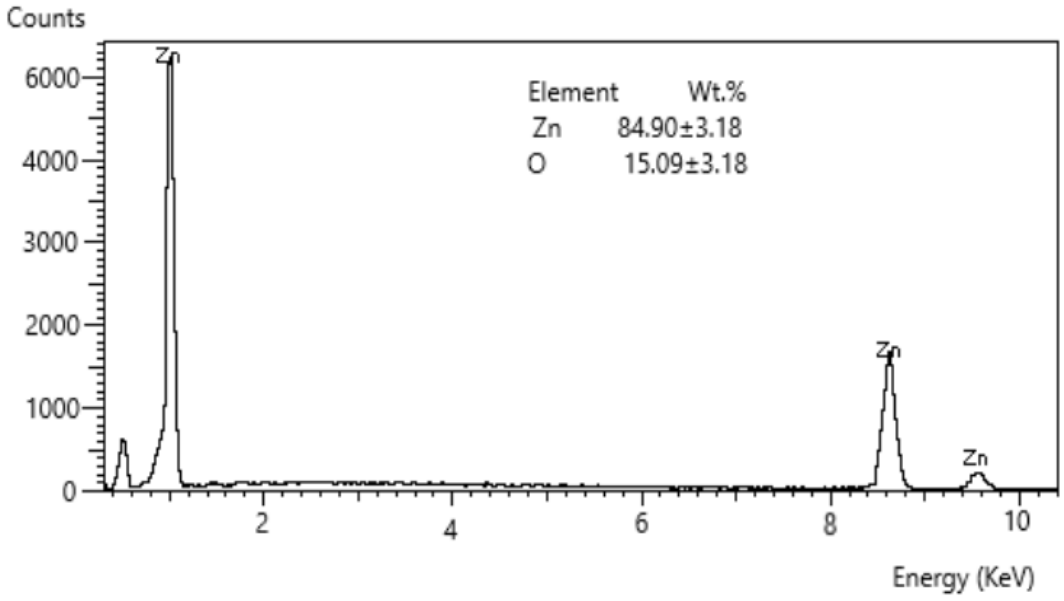
Counts
6000
4000
3000
2000
1000
0
Zn
Element Wt.%
Zn 84.90±3.18
O 15.09±3.18
Zn
Zn
2
4
6
8
10
Energy (KeV)

(a)

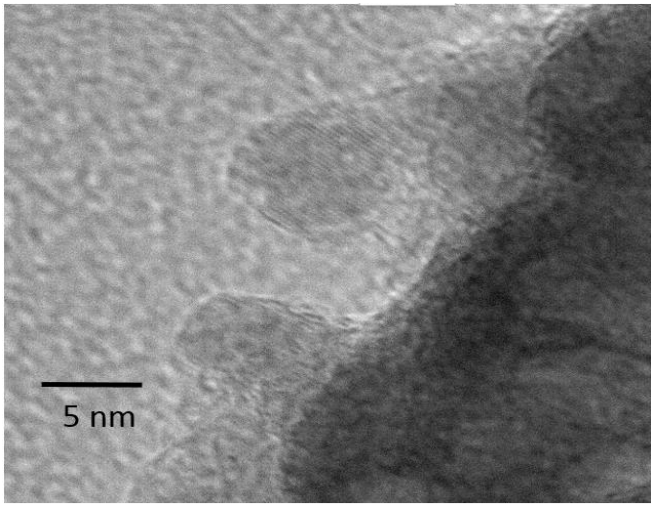
5 nm

(b)

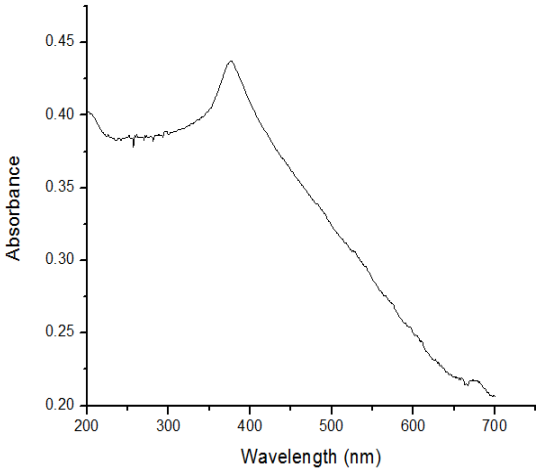
Absorbance
0.45
0.40
0.35
0.30
0.25
0.20
200
300
400
500
600
700
Wavelength (nm)

(c)

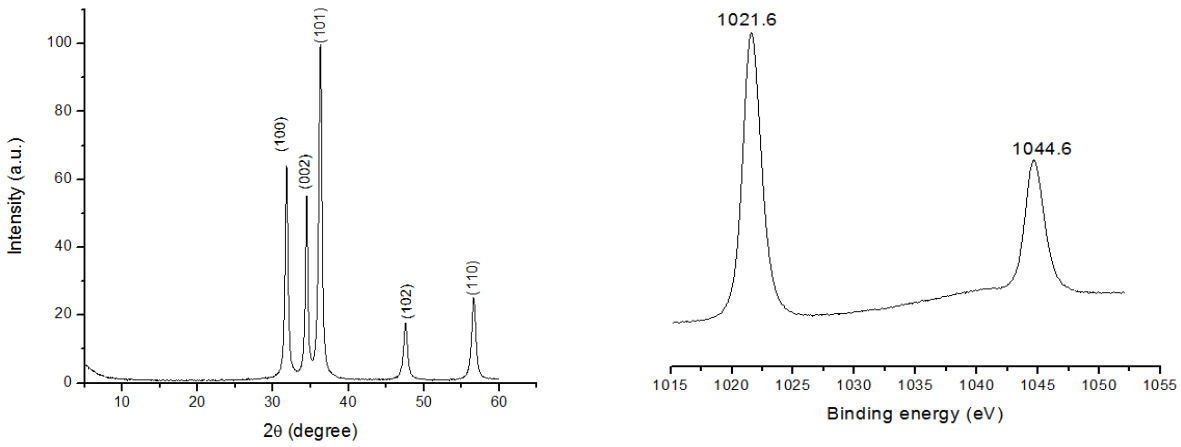

(d) (e)

Figure 4. EDS pattern and wt. (%) of each component: (a), TEM image (b), UV-Vis spectra (c), XRD diffraction pattern (d), and high resolution XPS spectrum for ZnO 2p (e), of ZnONPsAv.

3.2. NPs obtained by gamma irradiation reduction

3.2.1. AgNPsγ

EDS analysis shows no other weak signal, which indicates the purity (100%) of AgNPsγ (Figure 5a). As observed in TEM image (Figure 5b), the primary morphology of radiolytically synthesized Ag nanoparticles is spherical. This is the result of isotropic growth, while another small portion of NPs is hexagonal and caused by anisotropic growth. Crystal morphologies of the nanoparticles are determined by the rate of growth in different crystallographic directions. NP size can be controlled by experimental parameters which include reducing agent, pH, irradiation time (total dose) and dose rate irradiation. According to Singh et al. (2015) the appearance of anisotropic structures is attributed to a slow reaction rate, which reduces the quantity of nucleation sites to promote site-specific growth. Dose rate is a key factor to control the rate of reduction reaction of the metal ion. If a solution with the ion metallic species is irradiated with gamma rays at a low dose rate (as in this case), the generation of reducing agents is slower than the association of ions with atoms. As a consequence, the reduction process occurs preferentially on the surface of the aggregates (Belloni, 2006). The size distribution of the particles (Figure 5c) shows the polydispersity of the nanoparticles, ranging from 1 to 8 nm with a mean of 2.66 nm (±1.29). The UV-Vis spectra (Figure 5d) exhibit an absorption band at 380 - 450 nm, that corresponds to the surface plasmon absorption of Ag nanoparticles, similar to that reported by Sheikh et al. (2009). The X-ray diffraction reflections at 38.14° 2θ and 44.32° 2θ are typical of metallic silver particles (Figure 5e) (PDF 89-1397) and exhibit face-centered cubic (FCC) structure, in a similar way to when *Aloe vera* extract was used for the generation of these metallic nanoparticles. The high-resolution Ag 3d XPS spectrum (Figure 5f) presents two peaks at 368.4 eV and 374.4 eV. These belong to the Ag $3d_{5/2}$ and Ag $3d_{3/2}$ orbitals, respectively. The peak position, as well as the energy gap between these (6 eV), correspond with that from silver metal (Daiyan, Lu, Ng, & Amal, 2017).

3.2.2. CuNPsγ

EDS results confirm the presence of copper (96.72±0.72 wt. %) and oxygen (3.27±0.72 wt. %) in the Cu_2ONPsγ (Figure 6a). The SEM image shows well defined crystals with a geometrical figure, similar to tetrapod (Figure 6b), which may be because CuO sub-units attach to growing crystal faces, like tetrahedral. In addition, TEM image (Figure 6c) shows that the morphology of these nanoparticles is spherical with a mean diameter of 4.3 nm (±0.99), Figure 6d. Figure 6e, on the other hand, shows a bigger cluster. This fact can be explained by the use of a low radiation dose rate. Belloni (2006) observed that dose rate influences the rate of metal ion reduction. When the precursor is exposed to gamma radiation at a small dose rate, the generation of reducing radicals is lower than the combination of ions. Therefore, the process of the reduction happens principally on the surface of the obtained aggregates. It means that the reduction reaction of the ions does not participate in

the obtaining of new clusters. However, they could promote the growth of those already formed. Besides, the UV-Vis absorption peak (Figure 6f) at around 370 nm originates from Cu_2O nanoparticles. This is consistent with Salavati-Niasari and Davar (2009). The XRD peaks at 29.55° 2θ, 36.41° 2θ, 42.29° 2θ correspond to the (110), (111) and (200) planes of the Cu_2ONPs (PDF 05-0667) (Rehana et al., 2017), with a cubic crystal system. According to the pattern, there are no impurities (Figure 6g). XPS spectrum (Figure 6h), has characteristic Cu(II) $2p_{3/2}$ binding energy at 932.3 eV separated from Cu(II) $2p_{1/2}$ by 19.9 eV, which is similar to that reported by Biesinger (2017).

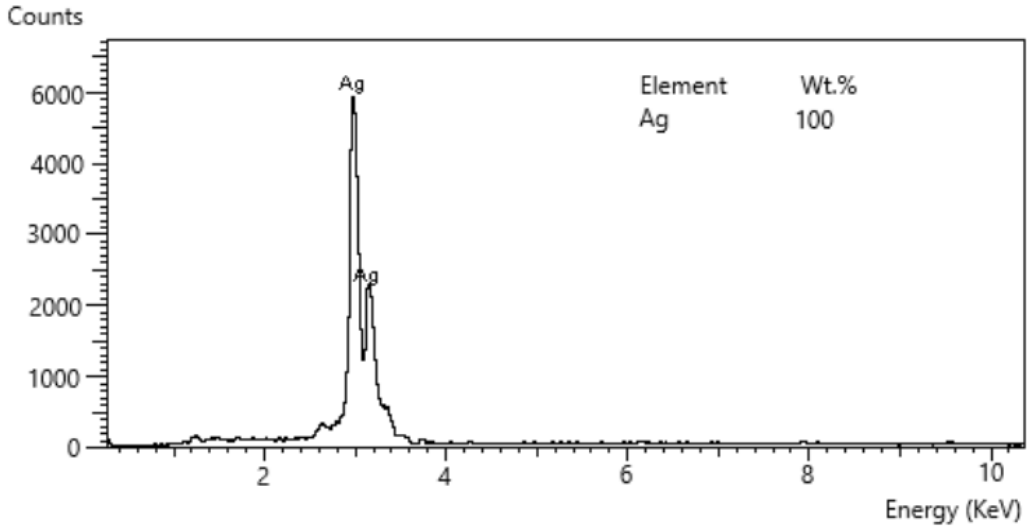

(a)

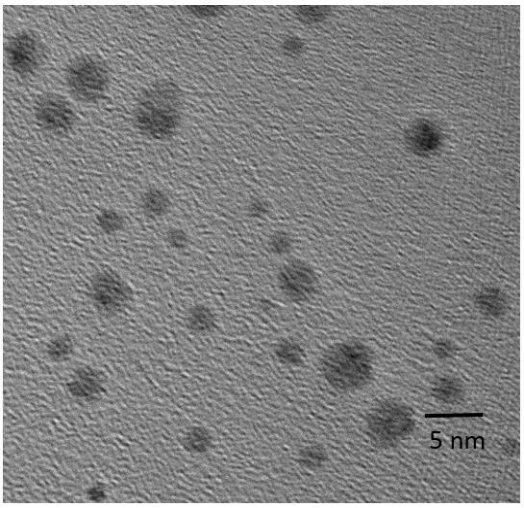

(b)

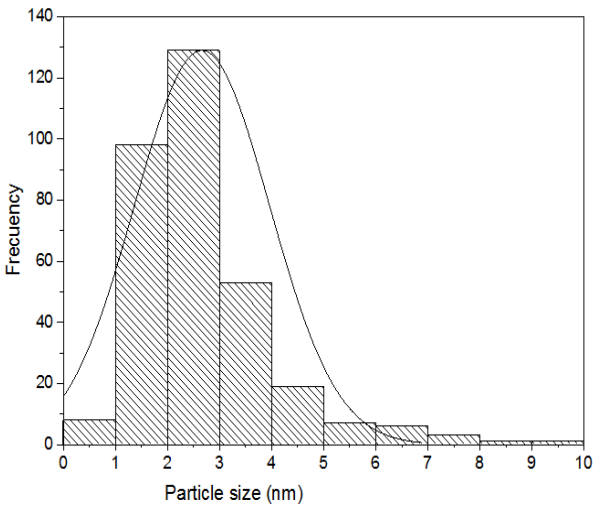

(c)

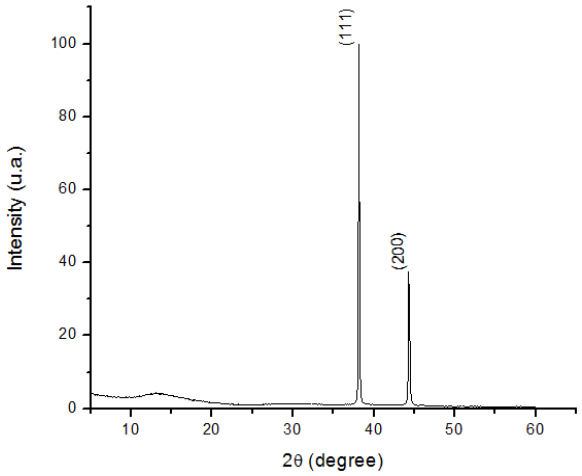

(d)

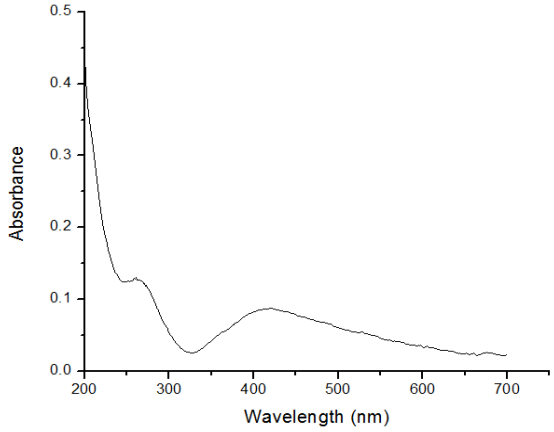

(e)

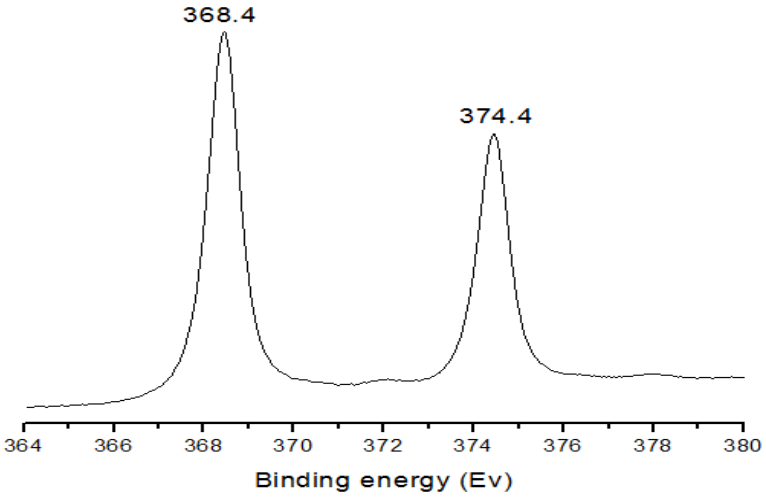

(f)

Figure 5. EDS pattern and wt. (%) of each component
(a), TEM image and histogram of distribution of particle size
(b, c), UV-Vis spectra (d), XRD diffraction pattern
(e), and high resolution XPS spectrum for Ag 3d (f), of AgNPsγ.

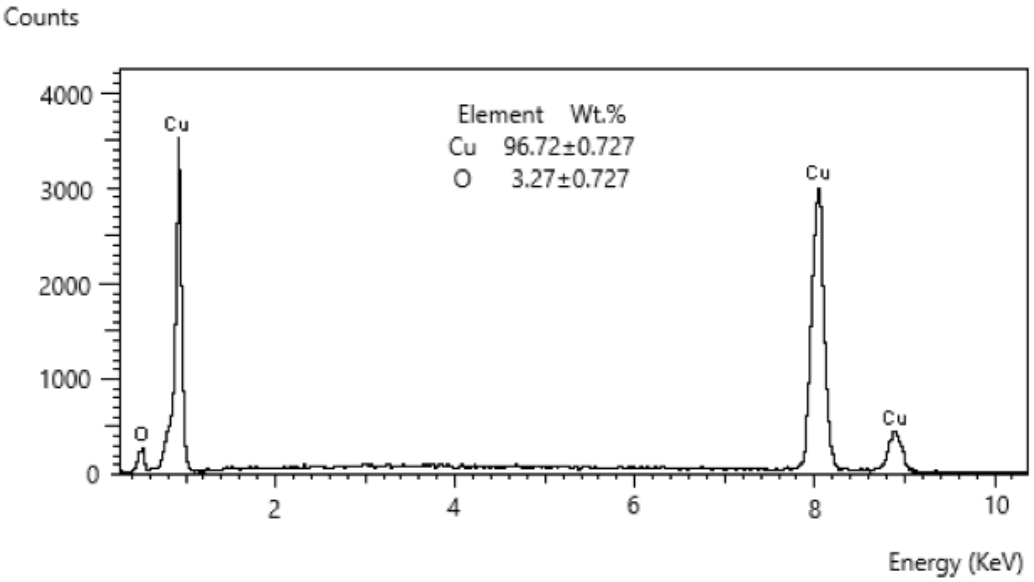
Counts
4000
3000
2000
1000
0
Cu
O
Element Wt.%
Cu 96.72±0.727
O 3.27±0.727
Cu
Cu
2
4
6
8
10
Energy (KeV)

(a)

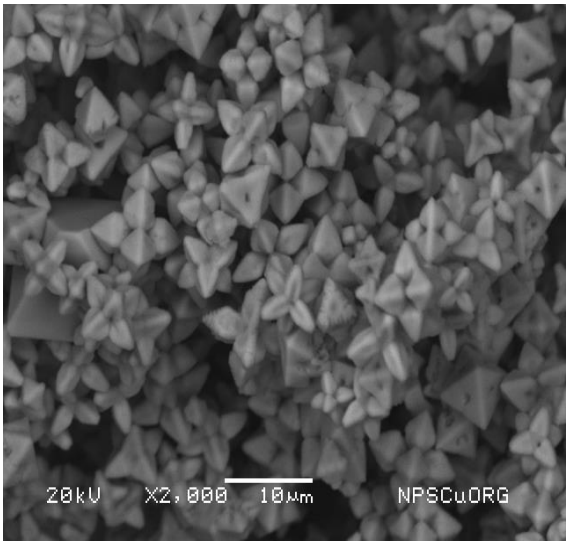
20kV X2,000 10µm NPSCuORG

(b)

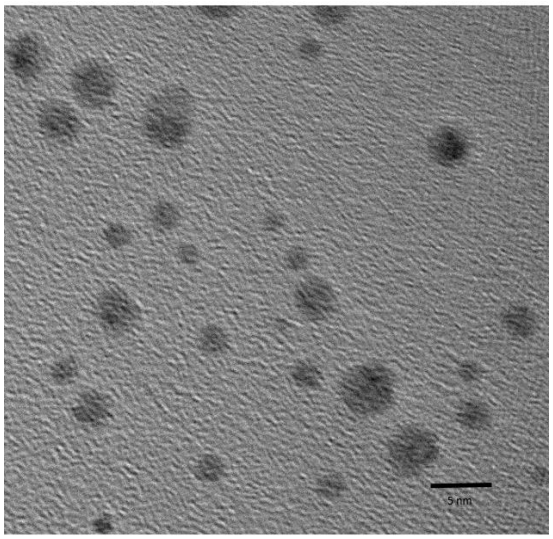

(c)

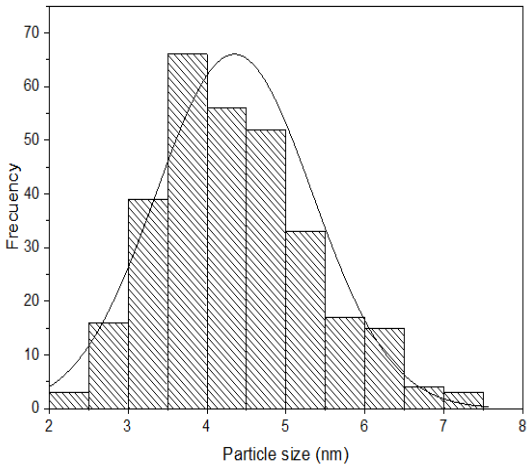
Frecuency
Particle size (nm)
0
10
20
30
40
50
60
70
2
3
4
5
6
7
8

(d)

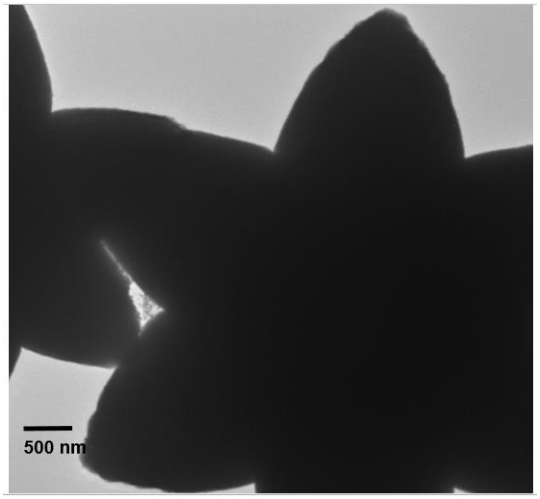
500 nm

(e)

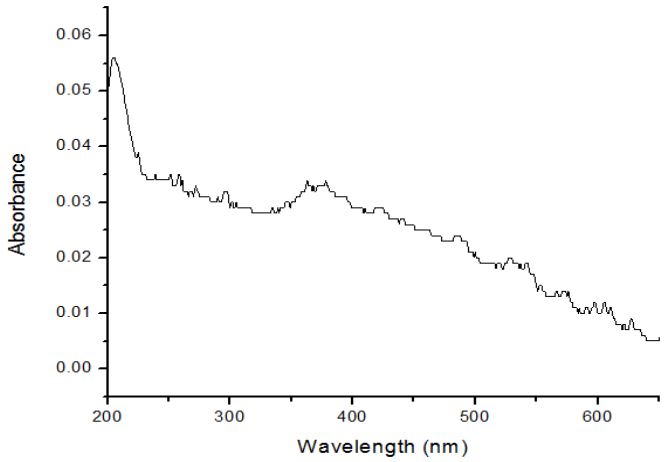
Absorbance
Wavelength (nm)
0.00
0.01
0.02
0.03
0.04
0.05
0.06
200
300
400
500
600

(f)

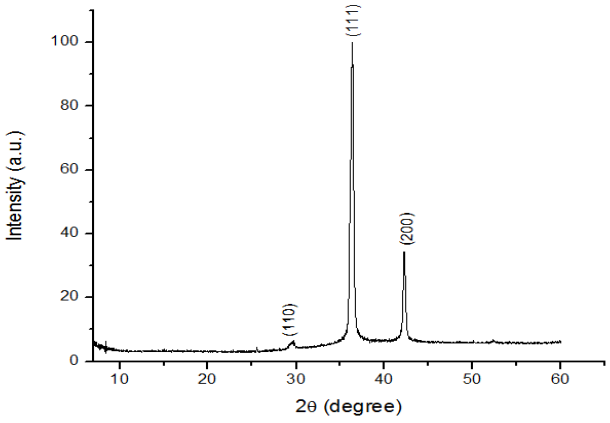
Intensity (a.u.)
2θ (degree)
(110)
(111)
(200)
0
20
40
60
80
100
10
20
30
40
50
60

(g)

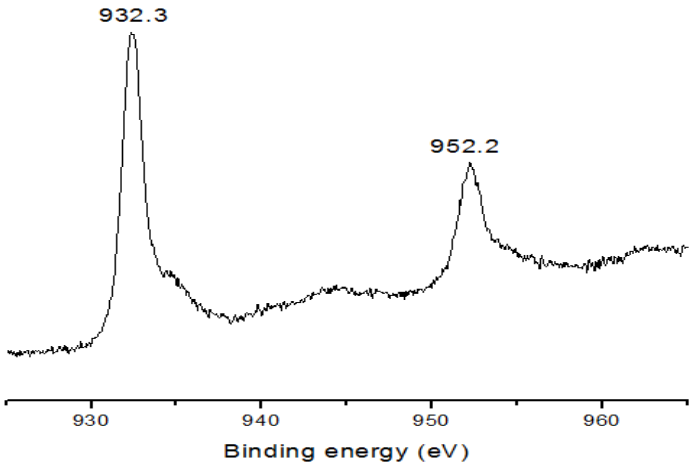

(h)

Figure 6. EDS pattern and wt. (%) of each component (a), SEM imagen (b), TEM image (c, e), and histogram of distribution of particle size (d), UV-Vis spectra (f), XRD diffraction pattern (g), and high resolution XPS spectrum for Cu 2p (h), of CuNPsγ.

3.2.3. Characteristics of metal and metal oxide nanoparticles obtained by a green synthesis or gamma irradiation

Table 1 shows the different characteristics of the Ag, Cu and Zn nanoparticles synthesized trough both *Aloe vera* and gamma irradiation routes. The chemical speciation of silver shows that Ag (0) is obtained using *Aloe vera* extract and gamma irradiation as reducing agents. The shape of the nanoparticles varies depending on the route of synthesis which is spherical when the extract of *Aloe vera* is used as reducing agent in contrast with spherical and hexagonal shapes when the gamma irradiation has interacted with the Ag(I) solution. The distribution of particle sizes has a greater amplitude for AgNPsAv (from 0 to 40 nm) than that found for AgNPsγ (from 0 to 10 nm). The mean particle size in these cases was 14 nm and 2.66 nm, respectively. For copper, the chemical speciation of the nanoparticles obtained varies according to the action of the reducer on the counterion of Cu(II) in solution. The contact of the $Cu(NO_3)_2$ with the *Aloe vera* extract favors the formation of CuO nanoparticles. When the same solution was exposed to gamma irradiation, nanoparticles were not obtained. However, when the $Cu(CH_3COO)_2$ was irradiated with a ^{60}Co gamma source, nanoparticles of Cu_2O were generated. This result confirms the importance of the counterion of Cu(II) in nanoparticle synthesis by gamma irradiation. The shape of the copper nanoparticles depends on the route of synthesis and these nanoparticles have a spherical form for CuNPsAv and spheres and clusters for CuNPsγ. The size range of the nanoparticles obtained from both synthesis routes is similar and the mean size was 6.93 nm for CuNPsAv and 4.34 nm for CuNPsγ. The chemical species obtained for the zinc nanoparticles was ZnO when the $Zn(NO_3)_2$ solution was in contact with the *Aloe vera* extract. The shape of these nanoparticles is spherical, with a mean size of 5 nm. In the particular case of Zn(II), it was not possible to generate the nanoparticles under the experimental condition of gamma irradiation even when the counterion was different from NO_3^-.

Table 1. Characteristics of metallic nanoparticles obtained by *Aloe vera* extract and gamma irradiation.

Synthesis route	Metallic nanoparticle	Precursor	Chemical speciation	Shape	Size range (nm)	Mean size (nm)
Aloe vera	AgNPsAv	$AgNO_3$	Ag(0)	Spherical	0-40	14.00 (±9.50)
	CuNPsAv	$Cu(NO_3)_2{\cdot}2.5H_2O$	CuO	Spherical	0-8	6.93 (±1.92)
	ZnNPsAv	$Zn(NO_3)_2{\cdot}\ 6H_2O$	ZnO	Spherical	Not obtained	5.0*
Gamma irradiation	AgNPsγ	$AgNO_3$	Ag(0)	Spherical and hexagonal	0-10	2.66 (±1.29)
	CuNPsγ	$Cu(CH_3COO)_2{\cdot}H_2O$	Cu_2O	Spherical and clusters	0-8	4.34 (±0.99)
	ZnNPsγ	$Zn(NO_3)_2{\cdot}\ 6H_2O$	Not obtained	Not obtained	Not obtained	Not obtained

There are several papers in the literature regarding the obtention of metallic or metal oxide nanoparticles using *Aloe vera* and other kinds of plants. This is known as "green synthesis". Furthermore, the formation of nanoparticles by gamma irradiation can be considered as a clean synthesis. In both synthesis routes, the advantage is that toxic by-products are not generated. Therefore, it is essential to take account that the characteristics of the nanoparticles (such as chemical speciation, shape, and size) will affect the adsorption properties as well as on their antimicrobial activity. For this reason, it is important to consider the experimental conditions for obtaining them. The silver nanoparticles discussed in this paper were synthetized with *Aloe vera* extract and showed similar chemical speciation and morphology to those obtained by Tippayawat, Phromviyo, Boueroy, and Chompoosor (2016). However, the sizes were smaller. When other types of plants were used, the size range obtained was wide (Table 2). With respect to the nanoparticles of copper, the chemical speciation (CuO) was similar to that observed by Gunalan, Sivaraj, and Venckatesh (2012). These authors modified the morphology of these nanoparticles using different amounts of the *Aloe vera* extract. The sizes of the CuO nanoparticles obtained in the present work were lower than those obtained by the same authors. The characteristics of the Cu nanoparticles obtained by way of other plant extracts vary in the chemical speciation, the morphology, and the size range. It is important to note that the precursors were $Cu(CH_3COO)_2$ or $CuSO_4$. In the case of this paper, it was $Cu(NO_3)_2$. The Zn nanoparticles obtained were similar in their chemical speciation to those obtained by Ali et al. (2016), while the morphology varied. The ZnO nanoparticles are smaller in size than those obtained by these authors. In comparison with the use of other plants for synthesis, the morphologies and the sizes of the generated nanoparticles were diverse.

The size of silver nanoparticles obtained by gamma irradiation was smaller than that obtained by green synthesis. This includes the *Aloe vera* extract. The morphology was spherical and hexagonal using gamma irradiation and plants. The chemical speciation was the same (Ag^o), independently of the route of the synthesis (Tables 1-3). The rate dose of irradiation used in the present work was 0.756 kGy/h, and Dhayagude, Das, Joshi, and Kapoor (2018) used 0.99 kGy/h (0.0165 kGy/min). In both cases, the same morphologies of the silver nanoparticles were observed. When the dose rate is higher than 0.7 kGy/h, only spherical morphologies were found (Table 3). It seems that the total dose did not influence this. However, the dose rate and total dose influenced the obtained particle size. Another factor that impacts on the characteristics of the silver nanoparticles obtained by gamma irradiation is the precursor. In the case of $AgClO_4$, the nanoparticles had a particle size larger than the precursor $AgNO_3$.

Table 2. Plants as reducing agents to obtain metallic or oxide metallic nanoparticles under different experimental conditions.

Variety	Metallic specie	Conditions	Chemical speciation	Morphology	Size nm	Reference
Aloe vera	Ag	$AgNO_3$ Extract of leaves Temperatures from 100 to 200 °C During 6 h or 12 h	Ag^o	Spherical	70-192 nm	(Tippayawat et al., 2016)
Azadirachta indica	Ag	$AgNO_3$ with aqueous leaf extract at room temperature for 24 h	Ag°	Spherical	40	(Ahmed, Saifullah, Ahmad, Swami, & Ikram, 2016)
Berberis vulgaris	Ag	$AgNO_3$ with aqueous extract for 1 h, room temperature	Ag°	Spherical	30 to 70	(Behravan et al., 2019)
Acacia catechu	Ag	$AgNO_3$ with aqueous extract 24 h room temperature	Ag°	Spherical	5-80	(Chand et al., 2020)
Aloe vera (*Aloe barbadensis Miller*	Cu	Leaf extract	CuO	The morphology of the nanoparticles can be controlled by tuning the amount of *Aloe vera* extract	15-30	(Gunalan et al., 2012)
Punica granatum	Cu	$Cu(CH_3COO)_2.H_2O$ with peels aqueous extract 10 min room temperature	Cu(II)	Spherical	10-100	(Ghidan et al., 2016)
Citrus medica	Cu	$CuSO_4$ with juice boiling temperature	Cu°	NS	10-60	(Shende, Ingle, Gade, & Rai, 2015)
Syzygium aromaticum	Cu	$Cu(CH_3COO)_2.H_2O$ with aqueous extract 15 min 30°C	Cu°	Spherical	12	(Rajesh, Ajitha, Reddy, Suneetha, & Reddy, 2018)
Aloe vera (Liliaceae)	Zn	Leaf extract	ZnO	Spherical, oval, hexagonal	8–20	(Ali et al., 2016)
Deverra tortuosa	Zn	Heated $Zn(NO_3)2.6H_2O$ over nigh with the aqueous extract	ZnO	Spherical	9 to 31	(Selim, Azb, Ragab, & Abd El-Azim, 2020)
Lycopersicon esculentum	Zn	Heated $Zn(NO_3)_2$ with juice at 80°C for 5 min	ZnO	Spherical	40 to 100	(Sutradhar & Saha, 2016)
Trifolium pratense	Zn	ZnO with flower powder 4 h 90°C, then 24 h 30°C	ZnO	Irregular	Agglomerated 100-190	(Dobrucka & Długaszewska, 2016)

The sizes of the copper oxide nanoparticles were smaller, and the morphology varied using a ^{60}Co source with respect to *Aloe vera* extract and the distribution of sizes were minor (Tables 2 and 3). The nanoparticles obtained by gamma irradiation presented a chemical speciation of Cu_2O and the speciation changed to CuO when the *Aloe vera* extract was used for synthesis. The precursor was not the same in both synthesis routes and this is a factor to be considered in the generation of the oxide copper nanoparticles. When the copper precursor was $CuSO_4$, Josi et al. (1998) found a chemical speciation of Cu^o and Ahmad, Ahmad, and Radiman (2009) observed two chemical speciation Cu^o and Cu(I). These differences can be attributed to dose rates (Table 3). In the case of the present work, the $Cu(CH_3COO)_2.H_2O$ was used as precursor in a similar way than Hori et al. (2014). These authors observed three different chemical species Cu^o, Cu(I) and Cu(II) with spherical shape. However, in the case of this work only one chemical species of nanoparticles was observed Cu(I) as Cu_2O, with spherical morphology. Nevertheless, clusters of copper were also presented. The distribution of the nanoparticles were between 0 and 8 nm using a dose rate of 0.756 kGy/h and when this dose increased to 4.7 kGy/h the interval of sizes increases from 2 to 60 nm (Table 3) as was reported in the literature (Hori et al., 2014).

The nanoparticles of zinc oxide were not obtained using $Zn(NO_3)_2 6H_2O$ as a precursor when they were submitted to a gamma irradiation field with a dose rate of 0.756 kGy/h and a total dose of 40 kGy.

Table 3. Gamma radiation as a reducing agent to obtain metal or metal oxide nanoparticles under different experimental conditions.

Source	Metallic specie	Conditions	Chemical speciation	Morphology	Size	Reference
^{60}Co	Ag	$AgNO_3$ Doses rate 1.2 kGy/h Total doses 30kGy Room temperature	Ag°	Spherical	10-25	(Gracien et al., 2019)
	Ag	$AgNO_3$ Doses rate 6 kGy/h Total doses 12kGy	Ag°	Spherical	3.6	(Rao et al., 2010)
	Ag	$AgClO_4$ Doses rate 0.0165 kGy/min	Ag°	Spherical (low total dose 0.5 kGy), Rectangular, pentagonal and hexagonal nanoplates (high total dose 4kGy)	15-60	(Dhayagude et al., 2018)
	Cu	$CuSO4.5H_2O$ Doses rate 25kGy/h	Cu°	Spherical	17-80	(Joshi, Patil, Iyer, & Mahumuni, 1998)
	Cu	$CuSO_4.5H_2O$ Doses rate 2kGy/h Total doses 100kGy	Cu°, Cu(I)	Spherical	2-10	(Ahmad et al., 2009)
	Cu	$Cu(CH_3COO)_2.H_2O$ Doses rate 4.7kGy/h Total doses 20kGy	Cu°, Cu(I), Cu(II)	Spherical	2-60	(Hori et al., 2014)

One of the most important properties of the metal or metal oxide nanoparticles is their ability to disinfect. Therefore, the microbicidal effect of these nanoparticles is related to the following characteristics: morphology, shape, and particle size, as was reported in the literature (Dizaj et al., 2014). Small nanoparticles (less than 30 nm) have the strongest bactericidal effect due to their capability of penetrating into bacterial cell wall and membrane, then, the positive surface charge of nanoparticles facilitates their binding to the negatively charged surface of the bacteria, causing membrane damage (Seil & Webster, 2012). Cheon, Kim, Rhee, Kwon, and Park (2019), report that the morphological dependence on antimicrobial activity of the NPs of Ag was, mainly, explained by total surface area and the number of Ag ions that were released.

4. Conclusions

The purity of the AgNPsγ is 100 % and its image reveals spherical and hexagonal shapes, with the appearance of anisotropic structures. AgNPsAv has 65.98 wt. % with the presence of other elements such as carbon, oxygen, magnesium, calcium and phosphorous. Also, AgNPsAv clearly show the presence of organic material capping the particles which are spherical in shape and vary in size. Regarding CuNPsAv, it presents 93.33% wt. % and oxygen 6.66% wt. in comparison to CuNPsγ with 96.72% wt. % and oxygen 3.27 wt. %. The synthesis of CuNPs by gamma irradiation produces bigger clusters by the different growth rates of bounding faces of their subunits to form geometrical figures. The metallic nanoparticles obtained through both *Aloe vera* and gamma irradiation methods show crystalline structure. Only in the case of the AgNPsAv phytochemical impurities are observed. The chemical speciation of the metallic species in both AgNPsAv and AgNPsγ is Ag(0), for CuNPsAv and CuNPsγ the Cu is observed as Cu(II) and Cu(I). In ZnNPsAv, the chemical speciation of Zn is Zn(II). It is not possible to obtain Zn nanoparticles under the experimental condition of this work by gamma irradiation. The precursor to obtaining copper nanoparticles and the experimental conditions from both synthetic methods determine the purity, morphology, crystallinity and chemical speciation of the metal.

The NPs generated by both methods are easily scaled up for production and suitable for several applications such as bactericidal agents, to name only one.

Acknowledgments

The authors are grateful to Mexican National Council for Science and Technology (CONACyT) for the financial assistance with the project No. 254665; ININ, for their support in carrying out the research work regarding TEM (I. Martínez), SEM and EDS (J. Pérez), XRD (P. López and L. Carapia) and XPS (R. Basurto) analysis as well as the permission to use the gamma irradiator (D. Ortiz); and to Facultad de Química (A. Colín).

Conflict of interest

The authors have no conflicts of interest to declare.

References

Ahamed, M., & Alhadlaq, H. (2014). Synthesis, Characterization, and Antimicrobial Activity of Copper Oxide Nanoparticles. *Journal of Nanomaterials, 10*(1155), 4. https://doi.org/10.1155/2014/637858

Ahmed, S., Ahmad, M., Swami, B. L., & Ikram, S. (2016). A review on plants extract mediated synthesis of silver nanoparticles for antimicrobial applications: A green expertise. *Journal of Advanced Research, 7*(1), 17–28. https://doi.org/10.1016/j.jare.2015.02.007

Ahmed, S., Saifullah, Ahmad, M., Swami, B. L., & Ikram, S. (2016). Green synthesis of silver nanoparticles using Azadirachta indica aqueous leaf extract . *Journal of Radiation Research and Applied Sciences, 9*(1), 1–7. https://doi.org/10.1016/j.jrras.2015.06.006

Ali, K., Dwivedi, S., Azam, A., Saquib, Q., Al-Said, M. S., Alkhedhairy, A. A., & Musarrat, J. (2016). *Aloe vera* extract functionalized zinc oxide nanoparticles as nanoantibiotics against multi-drug resistant clinical bacterial isolates. *Journal of Colloid and Interface Science, 472*, 145–156. https://doi.org/10.1016/j.jcis.2016.03.021

Alswat, A. A., Ahmad, M. B., & Saleh, T. A. (2017). Preparation and Characterization of Zeolite\Zinc Oxide-Copper Oxide Nanocomposite: Antibacterial Activities. *Colloids and Interface Science Communications, 16*, 19–24. https://doi.org/10.1016/j.colcom.2016.12.003

Baqer, A. A., Matori, K. A., Al-Hada, N. M., Kamari, H. M., Shaari, A. H., Saion, E., & Chyi, J. L. Y. (2018). Copper oxide nanoparticles synthesized by a heat treatment approach with structural, morphological and optical characteristics. *Journal of Materials Science: Materials in Electronics, 29*(2), 1025–1033. https://doi.org/10.1007/s10854-017-8002-3

Bashiri, A., Majid, R., Mahnaz, M., & Rad, M. (2018). Scalable , eco - friendly and simple strategy for nano - functionalization of textiles using immobilized copper - based nanoparticles. *Clean Technologies and Environmental Policy, 20*(9), 2119–2133. https://doi.org/10.1007/s10098-018-1596-1

Behravan, M., Hossein Panahi, A., Naghizadeh, A., Ziaee, M., Mahdavi, R., & Mirzapour, A. (2019). Facile green synthesis of silver nanoparticles using Berberis vulgaris leaf and root aqueous extract and its antibacterial activity. *International Journal of Biological Macromolecules, 124*, 148–154. https://doi.org/10.1016/j.ijbiomac.2018.11.101

Belloni, J. (2006). Nucleation, growth and properties of nanoclusters studied by radiation chemistry: Application to catalysis. *Catalysis Today, 113*(3–4), 141–156. https://doi.org/10.1016/j.cattod.2005.11.082

Biesinger, M. C. (2017). Advanced analysis of copper X-ray photoelectron spectra. *Surface and Interface Analysis, 49*(13), 1325–1334. https://doi.org/10.1002/sia.6239

Ahmad, S. I. B., Ahmad, M. S. B. H., & Radiman, S. B. (2009). A study on gamma irradiation synthesis of copper nanoparticles. *AIP Conference Proceedings, 1136*, 186–190. https://doi.org/10.1063/1.3160127

Brabazon, D., Pellicer, E., Zivic, F., Sort, J., Baró, M. D., Grujovic, N., & Choy, K. L. (Eds.). (2017). *Commercialization of Nanotechnologies–A Case Study Approach*. Springer. https://doi.org/10.1007/978-3-319-56979-6

Chand, K., Cao, D., Eldin Fouad, D., Hussain Shah, A., Qadeer Dayo, A., Zhu, K., … Dong, S. (2020). Green synthesis, characterization and photocatalytic application of silver nanoparticles synthesized by various plant extracts. *Arabian Journal of Chemistry.* https://doi.org/10.1016/j.arabjc.2020.01.009

Chandran, S. P., Chaudhary, M., Pasricha, R., Ahmad, A., & Sastry, M. (2006). Synthesis of gold nanotriangles and silver nanoparticles using Aloe vera plant extract. *Biotechnology Progress, 22*(2), 577–583. https://doi.org/10.1021/bp0501423

Cheon, J. Y., Kim, S. J., Rhee, Y. H., Kwon, O. H., & Park, W. H. (2019). Shape-dependent antimicrobial activities of silver nanoparticles. *International Journal of Nanomedicine, 14*, 2773–2780. https://doiorg/10.2147/IJN.S196472

Chikkanna, M. M., Neelagund, S. E., & Rajashekarappa, K. K. (2019). Green synthesis of Zinc oxide nanoparticles (ZnO NPs) and their biological activity. *SN Applied Sciences, 1*(1), 117. https://doi.org/10.1007/s42452-018-0095-7

Clifford, D. C., Castano, C. E., & Rojas, J. V. (2017). Supported transition metal nanomaterials: Nanocomposites synthesized by ionizing radiation. *Radiation Physics and Chemistry, 132*(December 2016), 52–64. https://doi.org/10.1016/j.radphyschem.2016.12.001

Daiyan, R., Lu, X., Ng, Y. H., & Amal, R. (2017). Highly Selective Conversion of CO2 to CO Achieved by a Three-Dimensional Porous Silver Electrocatalyst. *ChemistrySelect, 2*(3), 879–884. https://doi.org/10.1002/slct.201601980

Dhayagude, A. C., Das, A., Joshi, S. S., & Kapoor, S. (2018). γ-Radiation induced synthesis of silver nanoparticles in aqueous poly (N-vinylpyrrolidone) solution. *Colloids and Surfaces A: Physicochemical and Engineering Aspects, 556*, 148–156. https://doi.org/10.1016/j.colsurfa.2018.08.028

Dizaj, S. M., Lotfipour, F., Barzegar-Jalali, M., Zarrintan, M. H., & Adibkia, K. (2014). Antimicrobial activity of the metals and metal oxide nanoparticles. *Materials Science and Engineering C, 44*, 278–284. https://doi.org/10.1016/j.msec.2014.08.031

Dobrucka, R., & Długaszewska, J. (2016). Biosynthesis and antibacterial activity of ZnO nanoparticles using *Trifolium pratense* flower extract. *Saudi Journal of Biological Sciences, 23*(4), 517–523. https://doi.org/10.1016/j.sjbs.2015.05.016

El-Batal, A. I., El-Sayyad, G. S., El-Ghamery, A., & Gobara, M. (2017). Response Surface Methodology Optimization of Melanin Production by *Streptomyces cyaneus* and Synthesis of Copper Oxide Nanoparticles Using Gamma Radiation. *Journal of Cluster Science, 28*(3), 1083–1112. https://doi.org/10.1007/s10876-016-1101-0

Elumalai, K., Velmurugan, S., Ravi, S., Kathiravan, V., & Adaikala Raj, G. (2015). Bio-approach: Plant mediated synthesis of ZnO nanoparticles and their catalytic reduction of methylene blue and antimicrobial activity. *Advanced Powder Technology, 26*(6), 1639–1651. https://doi.org/10.1016/j.apt.2015.09.008

Elumalai, K., Velmurugan, S., Ravi, S., Kathiravan, V., & Ashokkumar, S. (2015). Bio-fabrication of zinc oxide nanoparticles using leaf extract of curry leaf (*Murraya koenigii*) and its antimicrobial activities. *Materials Science in Semiconductor Processing, 34*, 365–372. https://doi.org/10.1016/j.mssp.2015.01.048

Emam, H. E., El-Rafie, M. H., Ahmed, H. B., & Zahran, M. K. (2015). Room temperature synthesis of metallic nanosilver using acacia to impart durable biocidal effect on cotton fabrics. *Fibers and Polymers, 16*(8), 1676–1687. https://doi.org/10.1007/s12221-015-5197-x

Farzaneh, F., Asgharpour, Z., Nouroozi, F., & Haghshenas, S. (2017). Rapid Synthesis and Characterization of Zinc Oxide Nanoparticles with Albumen as Photodegradation of Congo Red Under Microwave Irradiation. *Journal of Cluster Science, 28*(3), 1637–1646. https://doi.org/10.1007/s10876-017-1175-3

Flores-Rojas, G. G., López-Saucedo, F., & Bucio, E. (2018). Gamma-irradiation applied in the synthesis of metallic and organic nanoparticles: A short review. *Radiation Physics and Chemistry*, *169*(August), 0–1. https://doi.org/10.1016/j.radphyschem.2018.08.011

Gerasimov, G. Y. (2011). Radiation methods in nanotechnology. *Journal of Engineering Physics and Thermophysics, 84*(4), 947–963. https://doi.org/10.1007/s10891-011-0554-0

Ghidan, A. Y., Al-Antary, T. M., & Awwad, A. M. (2016). Green synthesis of copper oxide nanoparticles using *Punica granatum* peels extract: Effect on green peach Aphid. *Environmental Nanotechnology, Monitoring and Management, 6*, 95–98. https://doi.org/10.1016/j.enmm.2016.08.002

Gracien, E. B., Jérémie, M. L., Joseph, L. K.-K., Omer, M. M., Antoine, M. K., Hercule, K. M., & Gerard, M. N. (2019). Role of hydroxyl radical scavenger agents in preparing silver nanoparticles under γ-irradiation. *SN Applied Sciences, 1*(9), 1–8. https://doi.org/10.1007/s42452-019-0973-7

Gunalan, S., Sivaraj, R., & Venckatesh, R. (2012). Aloe barbadensis Miller mediated green synthesis of mono-disperse copper oxide nanoparticles: Optical properties. Spectrochimica Acta - Part A: *Molecular and Biomolecular Spectroscopy, 97*, 1140–1144. https://doi.org/10.1016/j.saa.2012.07.096

Hajipour, M. J., Fromm, K. M., Akbar Ashkarran, A., Jimenez de Aberasturi, D., Larramendi, I. R. de, Rojo, T., … Mahmoudi, M. (2012). Antibacterial properties of nanoparticles. *Trends in Biotechnology, 30*(10), 499–511. https://doi.org/10.1016/j.tibtech.2012.06.004

Hori, T., Nagata, K., Iwase, A., & Hori, F. (2014). Synthesis of Cu nanoparticles using gamma-ray irradiation reduction method. *Japanese Journal of Applied Physics, 53*(5 SPEC. ISSUE 1), 2–6. https://doi.org/10.7567/JJAP.53.05FC05

Ingle, A. P., Duran, N., & Rai, M. (2014). Bioactivity, mechanism of action, and cytotoxicity of copper-based nanoparticles: A review. *Applied Microbiology and Biotechnology*. https://doi.org/10.1007/s00253-013-5422-8

Joshi, S. S., Patil, S. F., Iyer, V., & Mahumuni, S. (1998). Radiation induced synthesis and characterization of copper nanoparticles. *Nanostructured Materials, 10*(7), 1135–1144. https://doi.org/10.1016/S0965-9773(98)00153-6

Kamil Othman, N., Abdul Hamid, M. A., Saion, E., Abedini, A., & Daud, A. R. (2013). A review on radiation-induced nucleation and growth of colloidal metallic nanoparticles. *Nanoscale Research Letters, 8*(1), 1–10. https://doi.org/10.1186/1556-276x-8-474

Kasana, R. C., Panwar, N. R., & Kaul, R. K. (2017). *Nanoscience in Food and Agriculture 5* (Vol. 26). https://doi.org/10.1007/978-3-319-58496-6

Khodadadi, B., Bordbar, M., Yeganeh-Faal, A., & Nasrollahzadeh, M. (2017). Green synthesis of Ag nanoparticles/clinoptilolite using Vaccinium macrocarpon fruit extract and its excellent catalytic activity for reduction of organic dyes. *Journal of Alloys and Compounds, 719*, 82–88. https://doi.org/10.1016/j.jallcom.2017.05.135

Kumar, B., Angulo, Y., Smita, K., Cumbal, L., & Debut, A. (2016). Capuli cherry-mediated green synthesis of silver nanoparticles under white solar and blue LED light. *Particuology, 24*, 123–128. https://doi.org/10.1016/j.partic.2015.05.005

Kumar, B., Smita, K., Cumbal, L., Debut, A., & Angulo, Y. (2017). Biofabrication of copper oxide nanoparticles using Andean blackberry (Rubus glaucus Benth.) fruit and leaf. *Journal of Saudi Chemical Society, 21*, S475–S480. https://doi.org/10.1016/j.jscs.2015.01.009

Kumar, H., Venkatesh, N., Bhowmik , H. & Kuila, A. (2018). Metallic Nanoparticle: A Review. *Biomedical Journal of Scientific & Technical Research*, 4(2), 3765–3775. https://doi.org/10.26717/bjstr.2018.04.0001011

Kwon, J., Ducéré, J. M., Alphonse, P., Bahrami, M., Petrantoni, M., Veyan, J. F., … Chabal, Y. J. (2013). Interfacial chemistry in Al/CuO reactive nanomaterial and its role in exothermic reaction. *ACS Applied Materials and Interfaces, 5*(3), 605–613. https://doi.org/10.1021/am3019405

Lingaraju, K., Raja Naika, H., Manjunath, K., Basavaraj, R. B., Nagabhushana, H., Nagaraju, G., & Suresh, D. (2016). Biogenic synthesis of zinc oxide nanoparticles using Ruta graveolens (L.) and their antibacterial and antioxidant activities. *Applied Nanoscience (Switzerland), 6*(5), 703–710. https://doi.org/10.1007/s13204-015-0487-6

Logaranjan, K., Raiza, A. J., Gopinath, S. C. B., Chen, Y., & Pandian, K. (2016). Shape- and Size-Controlled Synthesis of Silver Nanoparticles Using Aloe vera Plant Extract and Their Antimicrobial Activity. *Nanoscale Research Letters, 11*(1). https://doi.org/10.1186/s11671-016-1725-x

Mahendiran, D., Subash, G., Arumai Selvan, D., Rehana, D., Senthil Kumar, R., & Kalilur Rahiman, A. (2017). Biosynthesis of Zinc Oxide Nanoparticles Using Plant Extracts of Aloe vera and Hibiscus sabdariffa: Phytochemical, Antibacterial, Antioxidant and Anti-proliferative Studies. *BioNanoScience, 7*(3), 530–545. https://doi.org/10.1007/s12668-017-0418-y

Mohanbaba, S., & Gurunathan, S. (2016). Differential biological activities of silver nanoparticles against gramnegative and gram-positive bacteria: A novel approach for antimicrobial therapy. Nanobiomaterials in Antimicrobial Therapy: *Applications of Nanobiomaterials.* Elsevier Inc. https://doi.org/10.1016/B978-0-323-42864-4.00006-3

Patil, B. N., & Taranath, T. C. (2018). Limonia acidissima L. leaf mediated synthesis of silver and zinc oxide nanoparticles and their antibacterial activities. *Microbial Pathogenesis, 115*, 227–232. https://doi.org/10.1016/j.micpath.2017.12.035

Rajesh, K. M., Ajitha, B., Reddy, Y. A. K., Suneetha, Y., & Reddy, P. S. (2018). Assisted green synthesis of copper nanoparticles using Syzygium aromaticum bud extract: Physical, optical and antimicrobial properties. *Optik, 154*, 593–600. https://doi.org/10.1016/j.ijleo.2017.10.074

Rao, Y. N., Banerjee, D., Datta, A., Das, S. K., Guin, R., & Saha, A. (2010). Gamma irradiation route to synthesis of highly re-dispersible natural polymer capped silver nanoparticles. *Radiation Physics and Chemistry, 79*(12), 1240–1246. https://doi.org/10.1016/j.radphyschem.2010.07.004

Rehana, D., Mahendiran, D., Kumar, R. S., & Rahiman, A. K. (2017). In vitro antioxidant and antidiabetic activities of zinc oxide nanoparticles synthesized using different plant extracts. *Bioprocess and Biosystems Engineering, 40*(6), 943–957. https://doi.org/10.1007/s00449-017-1758-2

Rojas, J. V., & Castano, C. H. (2012). Production of palladium nanoparticles supported on multiwalled carbon nanotubes by gamma irradiation. *Radiation Physics and Chemistry, 81*(1), 16–21. https://doi.org/10.1016/j.radphyschem.2011.08.010

Salavati-Niasari, M., & Davar, F. (2009). Synthesis of copper and copper(I) oxide nanoparticles by thermal decomposition of a new precursor. *Materials Letters, 63*(3–4), 441–443. https://doi.org/10.1016/j.matlet.2008.11.023

Seil, J. T., & Webster, T. J. (2012). Antimicrobial applications of nanotechnology: methods and literature The need for novel antibiotics. *International Journal of Nanomedicine, 7*, 2767–2781. https://doi.org/10.2147/IJN.S24805

Selim, Y. A., Azb, M. A., Ragab, I., & H. M. Abd El-Azim, M. (2020). Green Synthesis of Zinc Oxide Nanoparticles Using Aqueous Extract of Deverra tortuosa and their Cytotoxic Activities. *Scientific Reports, 10*(1), 1–9. https://doi.org/10.1038/s41598-020-60541-1

Sharma, P., Pant, S., Poonia, P., Kumari, S., Dave, V., & Sharma, S. (2018). Green Synthesis of Colloidal Copper Nanoparticles Capped with Tinospora cordifolia and Its Application in Catalytic Degradation in Textile Dye : An Ecologically Sound Approach. *Journal of Inorganic and Organometallic Polymers and Materials, 28*(6), 2463–2472. https://doi.org/10.1007/s10904-018-0933-5

Sharma, R., Dhillon, A., & Kumar, D. (2018). Mentha-Stabilized Silver Nanoparticles for High-Performance Colorimetric Detection of Al(III) in Aqueous Systems. *Scientific Reports, 8*(1), 1–13. https://doi.org/10.1038/s41598-018-23469-1

Sheikh, N., Akhavan, A., & Kassaee, M. Z. (2009). Synthesis of antibacterial silver nanoparticles by γ-irradiation. Physica E: Low-Dimensional *Systems and Nanostructures, 42*(2), 132–135. https://doi.org/10.1016/j.physe.2009.09.013

Shende, S., Ingle, A. P., Gade, A., & Rai, M. (2015). Green synthesis of copper nanoparticles by Citrus medica Linn. (Idilimbu) juice and its antimicrobial activity. *World Journal of Microbiology and Biotechnology, 31*(6), 865–873. https://doi.org/10.1007/s11274-015-1840-3

Siddiqi, K. S., ur Rahman, A., Tajuddin, & Husen, A. (2018). Properties of Zinc Oxide Nanoparticles and Their Activity Against Microbes. *Nanoscale Research Letters, 13*. https://doi.org/10.1186/s11671-018-2532-3

Singh, A. (2018). Zinc oxide nanoparticles: a review of their biological synthesis , antimicrobial activity , uptake , translocation and biotransformation in plants. *Journal of Materials Science, 53*(1), 185–201. https://doi.org/10.1007/s10853-017-1544-1

Singh, S., Bharti, A., & Meena, V. K. (2015). Green synthesis of multi-shaped silver nanoparticles: optical, morphological and antibacterial properties. *Journal of Materials Science: Materials in Electronics, 26*(6), 3638–3648. https://doi.org/10.1007/s10854-015-2881-y

Sricharussin, W., Threepopnatkul, P., & Neamjan, N. (2011). Effect of various shapes of zinc oxide nanoparticles on cotton fabric for UV-blocking and anti-bacterial properties. *Fibers and Polymers, 12*(8), 1037–1041. https://doi.org/10.1007/s12221-011-1037-9

Surjushe, A., Vasani, R., & Saple, D. (2008). Aloe vera: A short review. *Indian Journal of Dermatology, 53*(4), 163. https://doi.org/10.4103/0019-5154.44785

Sutradhar, P., & Saha, M. (2015). Synthesis of zinc oxide nanoparticles using tea leaf extract and its application for solar cell. *Bulletin of Materials Science, 38*(3), 653–657. https://doi.org/10.1007/s12034-015-0895-y

Sutradhar, P., & Saha, M. (2016). Green synthesis of zinc oxide nanoparticles using tomato (Lycopersicon esculentum) extract and its photovoltaic application. *Journal of Experimental Nanoscience, 11*(5), 314–327. https://doi.org/10.1080/17458080.2015.1059504

Tan, K. S., & Cheong, K. Y. (2013). Advances of Ag, Cu, and Ag-Cu alloy nanoparticles synthesized via chemical reduction route. *Journal of Nanoparticle Research*. https://doi.org/10.1007/s11051-013-1537-1

Tippayawat, P., Phromviyo, N., Boueroy, P., & Chompoosor, A. (2016). Green synthesis of silver nanoparticles in aloe vera plant extract prepared by a hydrothermal method and their synergistic antibacterial activity. *PeerJ, 2016(10)*, 1–15. https://doi.org/10.7717/peerj.2589

Tran, Q. H., Nguyen, V. Q., & Le, A. T. (2013). Silver nanoparticles: Synthesis, properties, toxicology, applications and perspectives. Advances in Natural Sciences: *Nanoscience and Nanotechnology, 4*(3). https://doi.org/10.1088/2043-6262/4/3/033001

Unser, S., Bruzas, I., He, J., & Sagle, L. (2015). Localized surface plasmon resonance biosensing: Current challenges and approaches. *Sensors (Switzerland), 15*(7), 15684–15716. https://doi.org/10.3390/s150715684

Venkatesh, K. S., Krishnamoorthi, S. R., Palani, N. S., Thirumal, V., Jose, S. P., Wang, F. M., & Ilangovan, R. (2015). Facile one step synthesis of novel TiO<inf>2</inf> nanocoral by sol–gel method using *Aloe vera* plant extract. *Indian Journal of Physics, 89*(5), 445–452. https://doi.org/10.1007/s12648-014-0601-8

Wang, F., & Hu, S. (2009). Electrochemical sensors based on metal and semiconductor nanoparticles. *Microchimica Acta, 165*(1-2), 1-22. https://doi.org/10.1007/s00604-009-0136-4

Wang, Y., Wang, D., Yan, B., Chen, Y., & Song, C. (2016). Fabrication of diverse CuO nanostructures via hydrothermal method and their photocatalytic properties. *Journal of Materials Science: Materials in Electronics, 27*(7), 6918–6924. https://doi.org/10.1007/s10854-016-4645-8

Watson, R. R., & Zibadi, S. (Eds.). (2013*). Bioactive dietary factors and plant extracts in dermatology* (p. 455). Humana Press. https://doi.org/10.1007/978-1-62703-167-7

Williams, K., Valencia, L., Gokulan, K., Trbojevich, R., & Khare, S. (2017). Assessment of antimicrobial effects of food contact materials containing silver on growth of Salmonella Typhimurium. *Food and Chemical Toxicology, 100*, 197–206. https://doi.org/10.1016/j.fct.2016.12.014

Yah, C. S., & Simate, G. S. (2015). Nanoparticles as potential new generation broad spectrum antimicrobial agents. DARU, *Journal of Pharmaceutical Sciences, 23*(1). https://doi.org/10.1186/s40199-015-0125-6

Yu, B., Wen, Y., Yang, X., & Cai, X. (2019). Synthesis of ZnO–Au composite microspheres by one-pot polyol method and its application as a photo-catalyst. *Journal of Materials Science: Materials in Electronics, 30*(1), 855–861. https://doi.org/10.1007/s10854-018-0356-7

Zhang, Y., Yang, D., Kong, Y., Wang, X., Pandoli, O., & Gao, G. (2010). Synergetic Antibacterial Effects of Silver Nanoparticles@Aloe Vera Prepared via a Green Method. *Nano Biomedicine and Engineering, 2*(4).
https://doi.org/10.5101/nbe.v2i4.p252-257

Zhu, J., Li, D., Chen, H., Yang, X., Lu, L., & Wang, X. (2004). Highly dispersed CuO nanoparticles prepared by a novel quick-precipitation method. *Materials Letters, 58*(26), 3324–3327.
https://doi.org/10.1016/j.matlet.2004.06.031